AIP | Applied Physics Letters

Evaluation of pulsed laser annealing for flexible multilayer MoS2 transistors

Hyuk-Jun Kwon, Sunkook Kim, Jaewon Jang, and Costas P. Grigoropoulos

Citation: Applied Physics Letters **106**, 113111 (2015); doi: 10.1063/1.4916131
View online: http://dx.doi.org/10.1063/1.4916131
View Table of Contents: http://scitation.aip.org/content/aip/journal/apl/106/11?ver=pdfcov
Published by the AIP Publishing

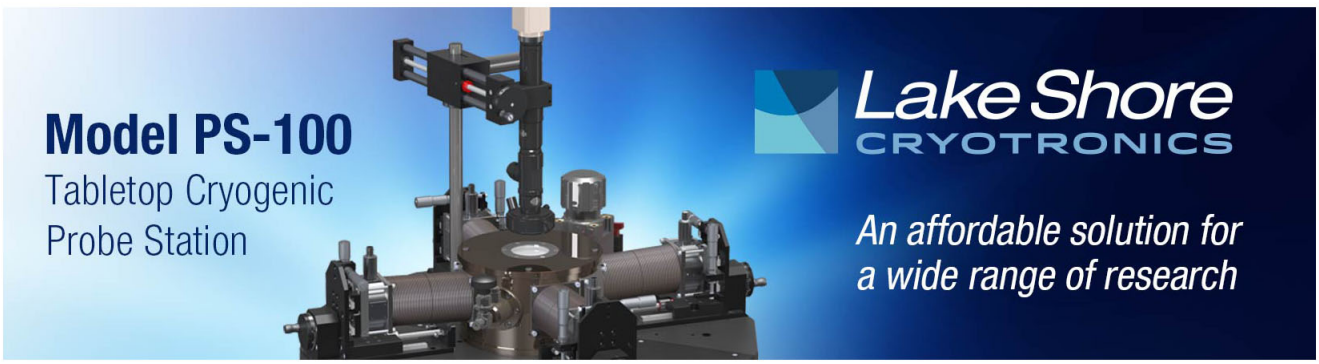

Evaluation of pulsed laser annealing for flexible multilayer MoS_2 transistors

Hyuk-Jun Kwon,[1,a)] Sunkook Kim,[2,a)] Jaewon Jang,[3,b)] and Costas P. Grigoropoulos[1,b)]
[1]*Department of Mechanical Engineering, University of California, Berkeley, California 94720-1740, USA*
[2]*Department of Electronics and Radio Engineering, Kyung Hee University, Yongin, Gyeonggi 446-701, South Korea*
[3]*Department of Electrical Engineering and Computer Sciences, University of California, Berkeley, California 94720, USA*

(Received 23 February 2015; accepted 11 March 2015; published online 20 March 2015)

To realize the proper electrical characteristics of field-effect transistors, the quality of the contact and interface must be improved because they can substantially distort the extracted mobility, especially for materials with low densities of states like molybdenum disulfide (MoS_2). We show that mechanically flexible MoS_2 thin-film transistors (TFTs) with selectively laser annealed source/drain electrodes achieve enhanced device performance without plastic deformation including higher field-effect mobility (from 19.59 to 45.91 $cm^2 V^{-1} s^{-1}$) in the linear regime, decreased subthreshold swing, and enhanced current saturation. Furthermore, numerical thermal simulations, measured current-voltage characteristics, and contact-free mobility extracted from the Y-function method suggest that the enhanced performance originated from a decrease in the Schottky barrier effect at the contact and an improvement of the channel interface. These results demonstrate that picosecond laser annealing can be a promising technology for building high performance flexible MoS_2 TFTs in flexible/stretchable circuitry, which should be processed at low temperatures. © *2015 AIP Publishing LLC*. [http://dx.doi.org/10.1063/1.4916131]

Flexible and stretchable electronics represent a critical frontier in the transformation of rigid, tabletop micro/nano electronics into portable, wearable systems that can be integrated into a variety of emerging technologies from sensing and monitoring to human-inspired applications.[1,2] Many conventional structures, materials, and processes are not compatible with flexible/stretchable device layouts. These requirements pose significant challenges that require a new, adaptive paradigm for the low-thermal budget (<100 °C) and functional components on a lightweight and inexpensive flexible platform. Displays are representative applications in the field of flexible/stretchable electronics.[3,4] Currently, users require new and more advanced displays for mobile phones, portable devices, and even televisions, with features including ultra-high resolution, higher frame rates (high driving speed), low power consumption, and larger size. Attaining such performance will require high-mobility transistors with low contact resistance (R_c).

In this regard, thin-film transistors (TFTs) based on a two-dimensional (2D) series of transition metal dichalcogenides (TMDs) with a formula of MX_2 (M = Mo, W; X = S, Se, Te), have attracted much attention as candidate materials to extend Si technology. This is due to their unique properties, especially for molybdenum disulfide (MoS_2), which include: high electron mobility at room temperature (~200 $cm^2 V^{-1} s^{-1}$), high I_{on}/I_{off} ratios (~10^7), relatively large bandgaps (1.2–1.9 eV), and mechanical flexibility (due to very thin atomic thickness, 6.5 Å).[5–7] Multilayer MoS_2 could have other advantages to improve the current drive of TFTs because multilayers can have a large density of states (DOS), make multiple conducting channels due to field effects, and provide stability in air.[8–10] Therefore, MoS_2 has been considered a channel material for high speed and/or flexible devices and a component material to improve the performance of conventional Si devices. Furthermore, for realizing high performance MoS_2 TFTs, we should consider metal-MoS_2 junctions, which are indispensable to the structure of TFTs, because non-ideal electric contacts on MoS_2 can form Schottky barriers at the junctions, and the undesirable contacts can hamper the inherent electrical characteristics of MoS_2. Therefore, to reduce the R_c and Schottky barrier, various efforts (doping, the use of scandium metal with a low work function, and thermal annealing) have been reported.[7,11,12] However, there are challenges and limitations to move forward in flexible electronics technologies. The chemical doping effect is gradually reduced over time. Moreover, scandium metals have been classified as a rare earth element and difficulties have been encountered in preparing them. The typically used flexible substrates (e.g., poly(ethylene naphthalate) (PEN), poly(ethylene terephthalate) (PET), and polyimide (PI)) have a low thermal budget (<200 °C). Therefore, high thermal annealing processes could lead to deformation in plastic substrates.

Unlike conventional thermal annealing, which affects the entire panel including unwanted areas in which the annealing process should be excluded, the irradiation of a pulsed laser with high energy density and short wavelength onto a metal electrode leads to the thermal annealing effect in a small, locally confined area that requires high temperature without extreme thermal damage.[13] Also, a laser enables the achievement of superb interfacial characteristics between metal and semiconducting material contact surfaces, resulting in reduced R_c and improved interfacial morphology.[14,15] However, in earlier studies, the laser annealing technique was only focused on the contacts even

[a)]H.-J. Kwon and S. Kim contributed equally to this work.
[b)]Authors to whom correspondence should be addressed. Electronic addresses: jaewonjang@berkeley.edu and cgrigoro@berkeley.edu.

though heat generated by laser absorption at the top surface could affect the channel interfaces by heat conduction. In this paper, we investigate the effects of picosecond pulsed laser annealing with a high-repetition rate (80 MHz) on both contacts and channel interfaces of flexible multilayer MoS_2 transistors. Here, we note that selective pulsed laser annealing induces enhanced electrical performance of flexible MoS_2 TFTs including a higher field-effect mobility (μ_{eff_lin}) of 45.91 $cm^2 V^{-1} s^{-1}$ in the linear regime, improved current saturation, and decreased subthreshold swing (SS). The numerical temperature analysis was expanded into the whole structure of the sample including the interfaces and exhibited the compatibility of our picosecond laser annealing with the flexible PEN substrate as well as the relatively high conducted heat (not to be ignored) at the channel interface. Furthermore, on the basis of the comparison between μ_{eff} and the intrinsic mobility (μ_0) extracted from the Y-function method (YFM) before and after laser annealing, we suggest that enhanced performance results from not only the improved contacts but also an increase in interface quality. Thus, the enhanced contact has a much greater effect than improving interface quality. Therefore, the pulsed laser annealing process suggests a future direction towards improving mobility in layered semiconductors.

Fig. 1(a) shows the schematic architecture of our flexible multilayer MoS_2 field-effect transistors (FETs) on the PEN substrate (DuPont Teijin Films, USA). For a bottom gate electrode, a 100-nm-thick indium thin oxide (ITO) was deposited on the PEN substrate at room temperature. Then, dual films (atomic-layer-deposited (ALD) Al_2O_3 of 50 nm/sputter-deposited SiO_2 of 250 nm) were formed as a gate dielectric layer. A MoS_2 flake with a thickness of ~50 nm was mechanically transferred from bulk MoS_2 crystals (SPI Supplies, USA) on the deposited dielectric layer. After that, Ti (10 nm) and Au (300 nm) were continuously deposited by electron-beam evaporation at room temperature. Finally, conventional UV photolithography and lift-off techniques allowed definition of the source and drain electrodes. Fig. 1(b) shows a proof-of-concept demonstration of a completely fabricated flexible multilayer MoS_2 FET rolled up in a curved shape and an optical microscope image from the top of the device (inset of Fig. 1(b)). A yttrium vanadate ($Nd:YVO_4$) picosecond pulsed laser having a wavelength of 355 nm, a pulse width based on full width at half maximum of 12 ps, and a pulse repetition rate of 80 MHz was applied for selectively focused annealing at the contact regions. Note that the shape of the pulsed laser beam was a Gaussian with a 1.5–μm beam diameter at a $1/e^2$ peak irradiance, and was obtained through a 39× objective lens with a numerical aperture (NA) of 0.5. Moreover, a computer simultaneously operated laser power, scan speed, position of the high-resolution x-y positioning stage, and optical shutter during the annealing process, as shown in Fig. 1(c).

The pulsed laser irradiated the edge of the contact region (between MoS_2 and metal contacts) and was scanned at a speed of 10 μm/s across the contacts (Fig. 2(a)) because charge injection mainly occurs from the edge of the metal electrodes into the semiconducting channels.[16] In addition, the temperature generated by the laser annealing did not cool down to below ambient temperature before the next pulse arrives due to the high repetition rate (80 MHz).[17] Heat accumulation effects have been shown to contribute to the annealing of MoS_2 FETs for flexible electronics.[14] To predict the generated heat and temperature distribution inside the sample, we computed the temperature with respect to the scanned time at three particular points (point 1 is the interface between contact and MoS_2, point 2 is the interface

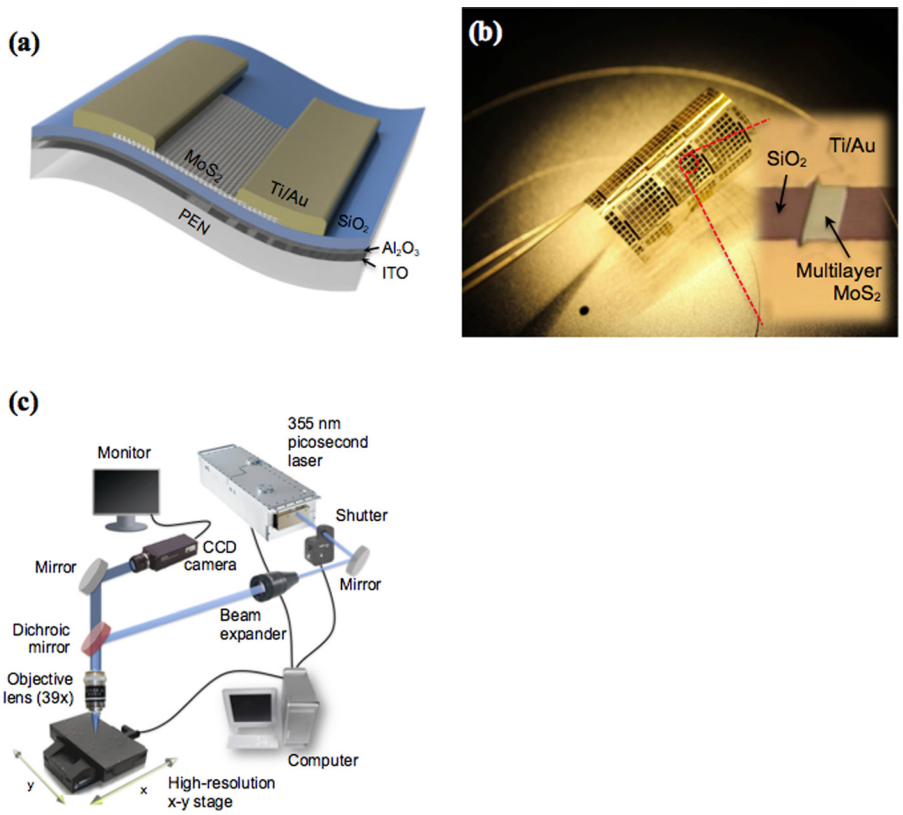

FIG. 1. Flexible multilayer MoS_2 FETs and pulsed laser annealing system. (a) Cross-sectional schematic structure of multilayer MoS_2 FETs with a 300-nm-thick SiO_2 gate dielectric. Picosecond laser irradiation with a Gaussian beam profile is focused and scanned along the edge of the source and drain electrodes. (b) Top-view of the optical microscope image for multilayer MoS_2 FETs after fabricating completely. (c) Schematic view of the optical setup for picosecond laser annealing.

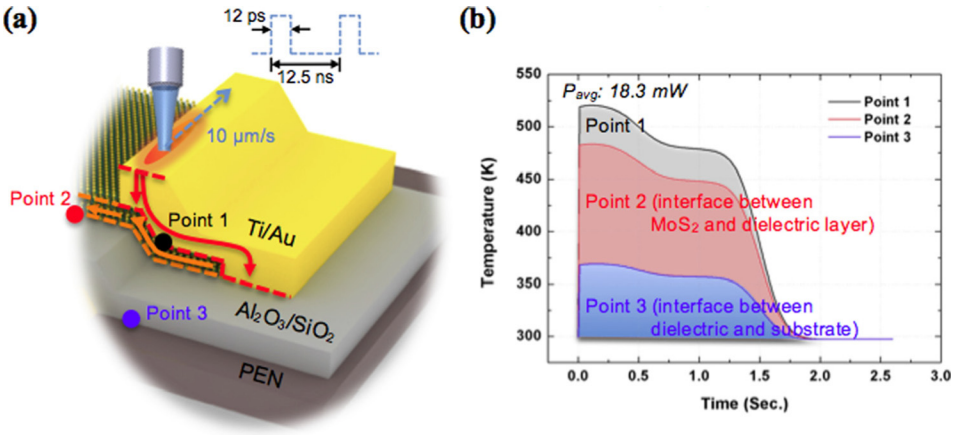

FIG. 2. Numerical thermal analysis of temperature distribution under a moving picosecond-pulsed laser source. (a) Spatial schematic images of laser-irradiated Au contacts at a speed of 10 μm/s on a flexible PEN substrate and three points of interest: point 1 (the interface between the contact and MoS_2), point 2 (the interface between MoS_2 and the dielectric layer), and point 3 (the interface between the dielectric layer and the substrate). (b) Predicted temperature distributions versus exposure time at the three specific points when a picosecond pulsed laser was applied and scanned onto the top surface (Au) at ambient conditions.

between MoS_2 and dielectric layer, and point 3 is the interface between the dielectric layer and substrate) through COMSOL Multiphysics as a picosecond pulsed laser source was applied under the experimental conditions explained above (Fig. 2(a)). We note that the equilibrium temperature approximation is adopted for reducing the computational cost, although this assumption overestimates the transient temperature in the picosecond time scale. However, the time required for laser annealing far exceeds the non-equilibrium state (before the electron and lattice temperatures equilibrate, ~40 ps). Furthermore, the prediction of heat accumulation effecting laser annealing does not differ from the classical Fourier conduction model below:

$$\rho C_p \frac{\partial T}{\partial t} - \nabla(\mathrm{k}\nabla \mathrm{T}) = Q(x, y, z), \tag{1}$$

where ρ is the density, C_p is the specific heat, k is the thermal conductivity, and Q is the Gaussian heat source term expressed as

$$Q(x, y, z) = Q_0(1 - R_c)\frac{A_c}{2\pi\sigma_x\sigma_y} e^{-\left[\frac{(x-x_0)^2}{2\sigma_x^2} + \frac{(y-y_0)^2}{2\sigma_y^2}\right]} \times e^{-A_c z}, \tag{2}$$

where Q_0, R_c, A_c, and $\sigma_{x,y}$ indicate the total input power, the reflectivity, the absorption coefficient, and the x,y widths of the spatial irradiation distribution, respectively.

As picosecond laser pulses were irradiated directly at the surface of the Au electrode the temperature dramatically increased in very short time periods (~12 ps), producing sharp temperature spikes. Before the pulsed laser source moved completely outside the targeted fixed point (~0.15 s), the temperature consisted of picosecond-duration spikes superposed on the continuous accumulated temperature field. After that, the effect of these high peaks faded, and the temperature of the top and bottom of the electrode merged due to heat conduction. Finally, the generated heat dissipated completely (~2.6 s). Fig. 2(b) shows the accumulated and conducted temperature (generated by absorption of the irradiated laser light at a power of 18.3 mW at the top surface as shown in Fig. 2(a)) with time at the three points. At point 1 (the interface between the contact and MoS_2), the generated temperature was around 533 K, which is high enough for effective laser annealing.[14] Furthermore, this heat reached around 480 K (~210 °C) at point 2 (the interface between MoS_2 and the dielectric layer). According to other reports, this temperature was not low enough to be ignored in respect to annealing.[7,8] Unfortunately, we were not able to obtain a direct measurement to confirm the effect on the interfaces. However, we sought to indirectly assess the impact on the interfaces using YFM as will be discussed later. The heat generated on the top surface of the Au could reach point 3 (the interface between the dielectric layer and the substrate). Nevertheless, the obtained temperature, 365 K (~90 °C), was below the glass transition temperature of the PEN substrate (~155 °C). Therefore, no thermal damage is expected after the laser process, in good agreement with the results of the laser experiments.

We examined the effect of laser annealing on the electrical performance of MoS_2 TFTs on flexible PEN substrates. Fig. 3(a) shows the log- (left) and linear-scale (right) drain current versus gate voltage (I_{ds}-V_{gs}) curves of representative MoS_2 TFTs with a channel length of 4.8 μm and width of 6 μm at a fixed low source-drain voltage ($V_{ds} = 1.0$ V) before (black dots) and after laser annealing (red dots) with an average laser power (P_{avg}) of 18.3 mW. Also, the drain current as a function of drain voltage (I_{ds}-V_{ds}) in a range from 0 to 30 V for the selected V_G (from −20 to +20 V in 5-V increments) was plotted, as shown in Fig. 3(b). At room temperature and in air, the as-fabricated MoS_2 TFT (before laser treatment) exhibited acceptable switching behavior (on/off current ratio, I_{on}/I_{off} of $\sim 1.99 \times 10^7$), a SS of ~4.05 V/decade, μ_{eff_lin} of ~19.59 $cm^2 V^{-1} s^{-1}$, typical n-type behavior with negative threshold voltages (V_{th}), and a normally on-state for the device. Following laser annealing, electrical performance was enhanced including output characteristics of: increased I_{on}/I_{off} of $\sim 2.70 \times 10^8$ without a change in I_{off}, reduced SS of ~3.06 V/decade, an improved μ_{eff_lin} of ~45.91 $cm^2 V^{-1} s^{-1}$ (over twice), and strong saturation at I_{ds}-V_{ds}.

Furthermore, as shown in Fig. 3(c), we observed a nonlinear output curve in a very low V_{ds} regime (from 0 to 0.1 V) due to the Schottky barrier between the MoS_2 and Ti/Au electrodes before the laser process. However, after laser annealing, the curve exhibited linear characteristics, indicating a Schottky to Ohmic contact transition. This can allow increased electrical conductivity of the interface through the reduction of R_c by reducing the barrier effect. To confirm the results, we will examine the effect of the laser annealing through the YFM.

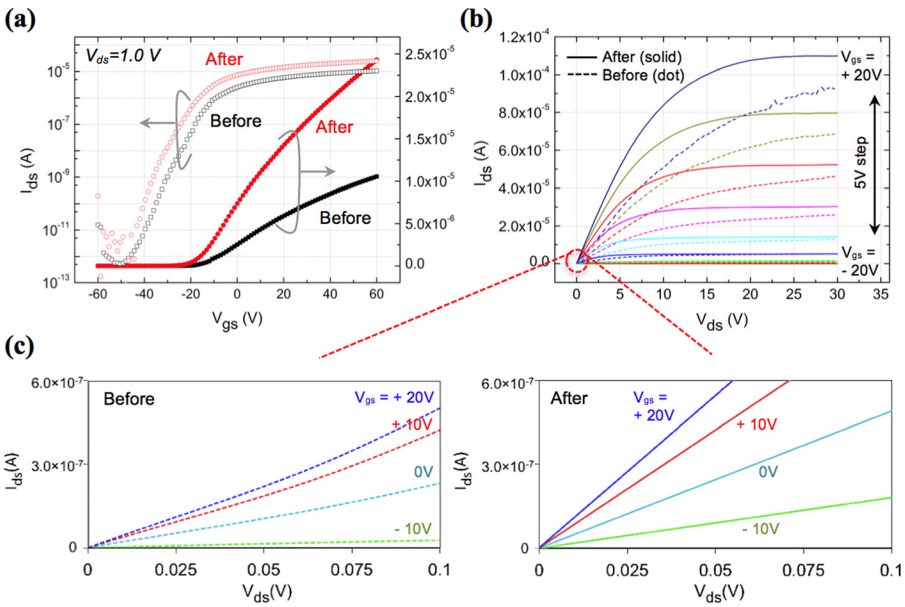

FIG. 3. Device performance of MoS_2 TFTs on flexible PEN substrates. (a) Transfer characteristics (I_{ds}-V_{gs}) for the flexible MoS_2 transistor in log-scale (left) and linear-scale (right) before and after laser annealing at $V_{ds} = 1$ V. (b) Output characteristics (I_{ds}-V_{ds}) before (dot) and after (solid) laser process. (c) Magnifications (before and after) for the low V_{ds} range from 0 to 0.1 V.

The field-effect mobility in the linear regime (μ_{eff_lin}) and the μ_0, which characterizes the maximum available mobility without a contact factor in the transistors, were estimated in order to understand the laser annealing impact on the contact conditions or MoS_2 channel layers of the fabricated devices. Normally, to extract the contact resistance of devices, the transfer-line method (TLM) is employed.[18] However, TLM requires several sets of transistors with various channel lengths and uniform contacts. Furthermore, TLM is quite demanding and difficult to apply in the case of the devices with arbitrary shapes and very small size channels. Due to this limitation, YFM has been proposed for the extraction of the low-field mobility without the influence of R_c (i.e., the intrinsic mobility, μ_0) and of other parameters (e.g., R_c, mobility attenuator factor (θ), V_{th}) as well.[19,20] Since there is no need to make specifically designed devices, the YFM could be a simple and powerful method.[21–23] The YFM is based on the I_{ds}-V_{gs} relation in the linear region, as below

$$I_{ds} = g_{ds} \times V_{ds} = \frac{W}{L} Q_{ch} \mu_{eff} \times V_{ds}, \tag{3}$$

where g_{ds} is the channel conductance, μ_{eff} is the effective mobility, and Q_{ch} is the channel charge per unit area. Then, we consider the θ ($=\theta_0 + \theta^*$), including the contribution from the channel interface (θ_0) and the contact resistance ($\theta^* = \mu_0 C_{ox} R_c W/L$). Therefore, the I_{ds} can be written as

$$I_{ds} = \frac{W}{L} C_{ox}(V_{gs} - V_{th}) \frac{\mu_0}{1 + \theta(V_{gs} - V_{th})} \times V_{ds}. \tag{4}$$

Considering the definition of the transconductance ($g_m = \partial I_{ds}/\partial V_{gs}$, $V_{ds} = const.$) and the μ_{eff} ($=L g_m/(W C_{ox} V_{ds})$), the Y function can be defined as

$$Y = \frac{I_{ds}}{\sqrt{g_m}} = \sqrt{\frac{W}{L} C_{ox} \mu_0 V_{ds}} \times (V_{gs} - V_{th}), \tag{5}$$

in order to eliminate θ. Note that Eq. (5) is independent of R_c, which is assumed to be constant. It can be seen from Eq. (5) that μ_0 could be extracted from the slope of the Y function, as shown in Fig. 4(a). Using slopes obtained before (5.9×10^{-4}) and after (6.6×10^{-4}) laser annealing, the values of μ_0 are extracted. Fig. 4(b) shows the comparison of the μ_0 and the peak μ_{eff} at the same V_{ds}, +1.0 V. Before the laser process, a large discrepancy (48.18%) exists between μ_0 ($37.80\,cm^2\,V^{-1}\,s^{-1}$) and μ_{eff_lin} ($19.59\,cm^2\,V^{-1}\,s^{-1}$). However, after laser annealing, the discrepancy (2.95%) is greatly reduced: μ_0 ($47.31\,cm^2\,V^{-1}\,s^{-1}$) and μ_{eff_lin} ($45.91\,cm^2\,V^{-1}\,s^{-1}$). To further investigate the laser effects, we extracted the values of θ and estimated R_c by the following equations:

$$g_m = \left.\frac{\partial I_D}{\partial V_G}\right|_{V_D = const.} = \frac{W}{L} C_{ox} \frac{\mu_0}{[1 + \theta(V_G - V_T)]^2} \times V_D. \tag{6}$$

For obtaining θ, Eq. (6) can be rewritten as

$$\frac{1}{\sqrt{g_m}} = \sqrt{\frac{1}{G_m V_D}} \{\theta(V_G - V_T) + 1\}, \tag{7}$$

where $G_m = (W/L)\mu_0 C_{ox}$ is the transconductance with the μ_0. From Eq. (7), the values of θ for as-fabricated (1.0×10^{-2}) and after laser annealing (6.3×10^{-3}) can be obtained by the linear fitted slopes (before: ~17 and after: ~9.6) of the $1/g_m^{0.5}$-V_G curve, as shown in Fig. 4(c). Through the known values of θ, the upper bound of R_c (R_{c_max}) can be calculated when we assume that the influence of θ_0 is negligible. Therefore, the contact effect mainly contributes to θ, and extracted values of R_{c_max} are 28.9 kΩ and 14.6 kΩ, respectively, before and after the laser process. Furthermore, μ_0 is slightly increased (20.10%) before and after the laser treatment. Since μ_0 is not affected by the contact factor, one of the possible reasons for this could be that the quality of the interface is enhanced. The traps between semiconductors and insulators play a critical role in determining the device performance, and the reduced interface trap concentrations were confirmed by the deceased SS values. To reconfirm the results, we roughly estimated the values of channel resistance (R_{ch}) by using the relation $R_{ch} = L/(\mu_0 W C_{ox}(V_G - V_{TH}))$ before and after laser annealing. The obtained values of R_{ch} were 85.34 kΩ (before) and 61.18 kΩ (after), respectively. The results of decreasing R_{ch} by the laser process support and

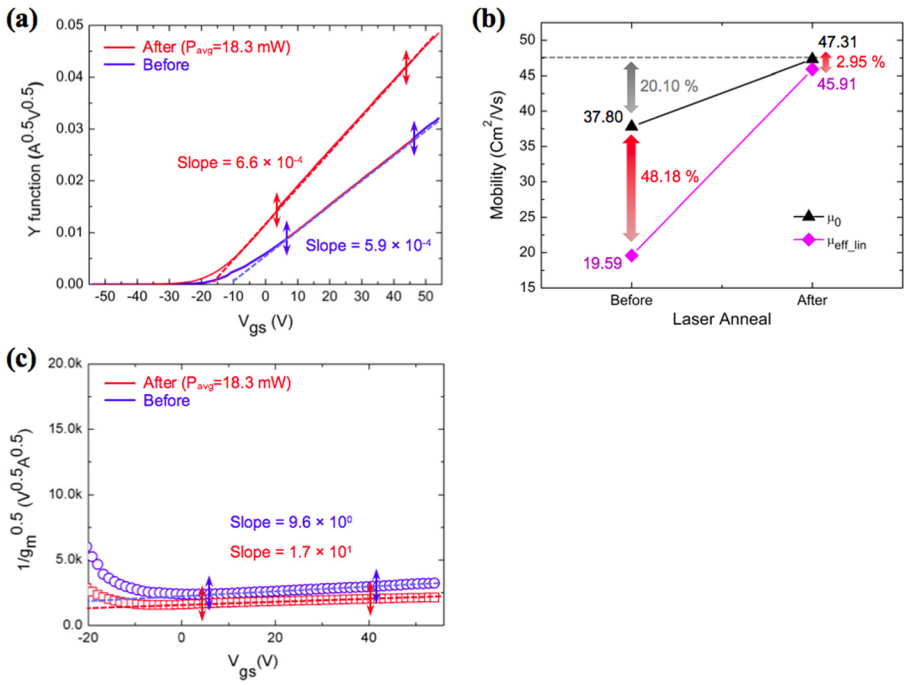

FIG. 4. Y function and evaluation of electrical parameters before and after the laser process. (a) Plots of Y function with respect to V_{gs} and the linear fitting in the strong accumulation region for obtaining the slope. (b) Comparison of the low-field mobility (μ_0) and peak field effect mobility (μ_{eff_lin}) before and after the laser process. (c) Plots of $1/g_m^{0.5}$ with respect to the V_{gs} and their slopes in the straight line fitting for extraction of the mobility attenuation factor (θ).

agree well with the enhanced interface conditions we described above. Also, through the comparison with R_{c_max} and R_{ch}, we have evidence that the diminishing discrepancy between the μ_{eff_lin} and μ_0 originates from the reduced contact and channel resistance by the laser annealing process. This indicates that the laser annealing process employed is the critical factor involved in enhancing the TFT performance by improving the contact conditions and promoting the interface quality without thermal damage to plastic substrates.

In summary, a high repetition ultra-short pulsed laser annealing process significantly enhanced the performance of flexible multilayer MoS_2 TFTs without inflicting thermal damage on plastic substrates. We employed an analysis of the extended temperature distribution through finite difference methods. The simulated results exhibited the compatibility of our picosecond laser annealing with the flexible substrate as well as improvement in contact with the channel interface. To estimate the laser annealing effect on device performance, YFM was used to extract R_c, μ_0, and the relationship between them. First, extracted SS values decreased. Second, μ_0 and μ_{eff_lin} were both increased. At the same time, the gap between R_c and R_{ch} and μ_0 and μ_{eff_lin} was substantially reduced. These data indicate an improvement of the interface quality between the MoS_2 channel and insulator. In addition, reduced contact barriers lead to a minimization in the resistance of major carrier injection and make it possible to approach the ideal μ_0 and μ_{eff_lin}. The employed laser annealing process is a powerful approach to enhance flexible MoS_2 TFT performance by reducing the contact resistance and promoting the interface quality without thermal damage to plastic substrates.

Support from the U.S. Air Force Office of Scientific Research AFOSR/AOARD under Grant No. FA2386-13-4123 was gratefully acknowledged. This research was also supported by the National Research Foundation of Korea (NRF-2013K1A3A1A32035549). In addition, we deeply appreciate the Lam Research Fellowship program for supporting H.-J.K.

[1]D. H. Kim, N. Lu, R. Ma, Y. S. Kim, R. H. Kim, S. Wang, J. Wu, S. M. Won, H. Tao, A. Islam, K. J. Yu, T. I. Kim, R. Chowdhury, M. Ying, L. Xu, M. Li, H. J. Chung, H. Keum, M. McCormick, P. Liu, Y. W. Zhang, F. G. Omenetto, Y. Huang, T. Coleman, and J. A. Rogers, Science **333**, 838 (2011).
[2]J. Viventi, D. H. Kim, J. D. Moss, Y. S. Kim, J. A. Blanco, N. Annetta, A. Hicks, J. L. Xiao, Y. G. Huang, D. J. Callans, J. A. Rogers, and B. Litt, Sci. Transl. Med. **2**, 24ra22 (2010).
[3]H. J. Kwon, H. Shim, S. Kim, W. Choi, Y. Chun, I. Kee, and S. Lee, Appl. Phys. Lett. **98**, 151904 (2011).
[4]S. Kim, H. J. Kwon, S. Lee, H. Shim, Y. Chun, W. Choi, J. Kwack, D. Han, M. Song, S. Kim, S. Mohammadi, I. Kee, and S. Y. Lee, Adv. Mater. **23**, 3511 (2011).
[5]K. F. Mak, C. Lee, J. Hone, J. Shan, and T. F. Heinz, Phys. Rev. Lett. **105**, 136805 (2010).
[6]A. Splendiani, L. Sun, Y. B. Zhang, T. S. Li, J. Kim, C. Y. Chim, G. Galli, and F. Wang, Nano Lett. **10**, 1271 (2010).
[7]B. Radisavljevic, A. Radenovic, J. Brivio, V. Giacometti, and A. Kis, Nat. Nanotechnol. **6**, 147 (2011).
[8]S. Kim, A. Konar, W. S. Hwang, J. H. Lee, J. Lee, J. Yang, C. Jung, H. Kim, J. B. Yoo, J. Y. Choi, Y. W. Jin, S. Y. Lee, D. Jena, W. Choi, and K. Kim, Nat. Commun. **3**, 1011 (2012).
[9]H. J. Kwon, H. Kang, J. Jang, S. Kim, and C. P. Grigoropoulos, Appl. Phys. Lett. **104**, 083110 (2014).
[10]H. J. Kwon, J. Jang, S. Kim, V. Subramanian, and C. P. Grigoropoulos, Appl. Phys. Lett. **105**, 152105 (2014).
[11]H. Fang, S. Chuang, T. C. Chang, K. Takei, T. Takahashi, and A. Javey, Nano Lett. **12**, 3788 (2012).
[12]S. Das, H. Y. Chen, A. V. Penumatcha, and J. Appenzeller, Nano Lett. **13**, 100 (2013).
[13]N. Misra, L. Xu, Y. L. Pan, N. Cheung, and C. P. Grigoropoulos, Appl. Phys. Lett. **90**, 111111 (2007).
[14]H. J. Kwon, W. Choi, D. Lee, Y. Lee, J. Kwon, B. Yoo, C. P. Grigoropoulos, and S. Kim, Nano Res. **7**, 1137 (2014).
[15]J. Kwon, Y. K. Hong, H. J. Kwon, Y. J. Park, B. Yoo, J. Kim, C. P. Grigoropoulos, M. S. Oh, and S. Kim, Nanotechnology **26**, 035202 (2015).
[16]F. Leonard and A. A. Talin, Nat. Nanotechnol. **6**, 773 (2011).
[17]S. M. Eaton, H. B. Zhang, and P. R. Herman, Opt. Express **13**, 4708 (2005).
[18]D. K. Schroder, *Semiconductor Material and Device Characterization*, 3rd ed. (Wiley, Piscataway, NJ, 2006).
[19]G. Ghibaudo, Electron. Lett. **24**, 543 (1988).
[20]G. Ghibaudo, Phys. Status Solidi A **113**, 223 (1989).
[21]Y. Xu, T. Minari, K. Tsukagoshi, J. A. Chroboczek, and G. Ghibaudo, J. Appl. Phys. **107**, 114507 (2010).
[22]H. Y. Chang, W. N. Zhu, and D. Akinwande, Appl. Phys. Lett. **104**, 113504 (2014).
[23]J. Na, M. Shin, M. K. Joo, J. Huh, Y. J. Kim, H. J. Choi, J. H. Shim, and G. T. Kim, Appl. Phys. Lett. **104**, 233502 (2014).